We are IntechOpen, the world's leading publisher of Open Access books
Built by scientists, for scientists

4,800
Open access books available

122,000
International authors and editors

135M
Downloads

154
Countries delivered to

Our authors are among the

TOP 1%
most cited scientists

12.2%
Contributors from top 500 universities

CLARIVATE ANALYTICS
BOOK CITATION INDEX
INDEXED

WEB OF SCIENCE™

Selection of our books indexed in the Book Citation Index
in Web of Science™ Core Collection (BKCI)

Interested in publishing with us?
Contact book.department@intechopen.com

Thermophysical Properties of Metal Oxides Nanofluids

Zafar Said and Rahman Saidur

Additional information is available at the end of the chapter

Abstract

Thermophysical properties of TiO_2, Al_2O_3 and SiO_2 nanofluids are experimentally investigated and compared with published data. Density has been measured over a range of 25–40°C for nanoparticle volumetric concentration of 0.05–4%. Viscosity experiments were carried out over a wide temperature range, from 25 to 80°C, to determine their applicability in such ranges. Nanofluids with particle volume fraction ranging from 0.02 to 0.03% and 1–4 kg/min were examined for the convective heat transfer and pumping power. The heat transfer coefficient of the nanofluid rises with rising mass flow rate, as well as rising volume concentration of metal oxide nanofluids; however, increasing the volume fraction results in increasing the density and viscosity of nanofluid, leading to a slight increase in friction factor which can be neglected. Addition of surfactants results in part of the increment in viscosity as well. An empirical formula for density is proposed, which also contributes to the novelty of this paper.

Keywords: nanofluids, surfactants, density, viscosity, pressure drop, heat transfer coefficient

1. Introduction

Thermophysical properties of nanofluids are significant to enhance the heat transfer behaviour. It is tremendously significant in controlling industrial and energy saving prospects. Great interest has been shown by the industry in nanofluids. Unlike conventional particle-fluid suspension (millimetre- and micrometre-sized particles), nanoparticles have great ability to enhance the thermal transport properties. In the last decade, due to the ability of improving thermal properties, nanofluids have gained prominent attention. Based on the broad research, it has been recognized that the suspension of metallic particles in a base fluid significantly increases the thermal conductivity of the mixture [1], therefore improving the heat transfer capability. Such observations have inspired the industrial as well as the science community to

discover the thermophysical properties of nanofluids, such as density, viscosity, thermal conductivity and heat capacity. Obtaining the viscosity of nanofluids is of importance for establishing sufficient pumping power. Besides, the convective heat transfer coefficients, Prandtl and Reynolds numbers, are also reliant on viscosity.

The available literature has suggested that the nanofluids tend to enhance the heat transfer performance, most importantly the heat transfer coefficient, thermal conductivity and viscosity, which in turn affects the pumping power. Das et al. [2] experimentally showed that thermal conductivity of a nanofluid can be augmented up to fourfold by increasing temperature. Xuan and Li [3] also found that heat transfer coefficient could be enhanced by the use of nanofluids, particularly when increasing the flow or nanoparticle concentration.

Different results on the density of nanofluids have been reported by the researchers, most of which are for a particular temperature or for a particular nanofluid [4–12]. There is no generalized method or model to obtain the density of different nanofluids theoretically. Density of the nanofluids strongly depends on nanoparticle material and increases with the increase in volume concentration. Base fluid also plays a significant role in the density of the nanofluids, whereas the other parameters such as nanoparticles shape, size, zeta potential and additives do not affect the density of the nanofluids. For engineering applications, larger density is more preferable [13]. The equation for the density of two phase mixtures for particles of micrometre size is available in the literature for slurry flows [14]. Densities of solids are greater than that of the liquids, with the increase in the concentration of nanoparticles in the fluid, and the density of the nanofluid is found to increase. Density of the nanofluids is proportional to the volume ratio of nanoparticles (solid) and base fluid (liquid) in a system. Pak and Cho [15] conducted an experiment at one temperature (25°C) for Al_2O_3 and TiO_2 nanofluids of up to 4 vol.%.

Studies on viscosity have been reported by numerous researchers. Several researchers [16–19] observed a Newtonian behaviour in TiO_2-ethylene glycol, Al_2O_3-water, single wall carbon nanohorns (SWCNH)-water and TiO_2-water nanofluids, respectively. With the increase in particle concentration, increase in the viscosity is noted. Timofeeva et al. [20] observed that viscosity decreases with the increase in particle size; however, Pastoriza-Gallego et al. [21] observed a different behaviour. A non-Newtonian behaviour was found by other researchers. Some authors have also developed models to describe the rheological behaviour of nanofluids. Koo [22] introduced a model to predict the thermal conductivity and viscosity of nanofluid in terms of nanoparticle size, concentration and density. Masoumi et al. [23] also presented a model to calculate the effective viscosity by considering the Brownian motion and the relative viscosity between the fluid and particles.

Pumping power is deserted in more than a few studies although it directly effects the usefulness of the fluid in applications. This is due to the reason that heat transfer coefficients could be enhanced by merely increasing the flow velocity of the fluid, which results in additional pumping power due to the surged pressure losses. Any effort to improve heat transfer results in improved pressure losses. Also with the addition of nanoparticles to the base fluid, an antagonism between heat transfer growth and enhanced pressure losses is present. Hence, the real measure of efficiency of a heat transfer fluid is not only the convective heat transfer

coefficient alone, but also the pressure losses need to be taken into account for calculations as well [24]. Heat transfer of a nanofluid flow which is squeezed between parallel plates is investigated analytically using homotopy perturbation method (HPM). It was reported from the findings that the Nusselt number has a direct relationship with the nanoparticle volume fraction, the squeeze number and Ecket number when two plates are separated, but an inverse effect is noted when the plates are squeezed [25]. In another study, heat and mass transfer characteristics of unsteady nanofluid flow between two parallel plates are investigated considering thermal radiation. Ordinary differential equations are solved numerically using the fourth-order Runge-Kutta method. Results indicated that the radiation parameter increased with the concentration boundary layer thickness. It was also reported that the Eckert number, Schmidt number, squeeze parameter and radiation parameter have direct relationship with Nusselt number [26].

For nanofluids to be applied for practical applications, it is essential to study the effect of these nanofluids on the flow features and their effect on the pumping power and pressure drop, in addition to heat transfer performance enhancement. Calculations are carried out for different volume fractions of nanoparticles and for changing mass flow rate. The effectiveness of nanofluids is investigated by comparing the required pumping power of oxides nanofluids and the base fluid. The reason these oxides are considered for this study is that they are easy to produce and cheaper compared to the CNTs and graphene.

On the basis of the inclusive literature review, the main objectives of this study are to examine the effects of nanofluids on the density, viscosity, the pressure drop and the convection heat transfer characteristics. The nanofluids contained Al_2O_3, SiO_2, and TiO_2 nanoparticles in water as a base fluid. The analyses were done for several nanofluids and then associated them with the water as the base fluid. The potential outcomes and their details were also described.

2. Methodology

2.1. Materials

Deionized water was used as the base fluid. The nanoparticles (TiO_2, P25 ≥ 99.5% trace metals basis), (SiO_2, 99.5% trace metals basis) and (Al_2O_3, 99.8% trace metals basis) were purchased from Sigma-Aldrich. Sodium dodecyl sulphate (SDS, 92.5–100.5%, Sigma-Aldrich), polyvinyl-pyrrolidone (PVP, Sigma-Aldrich), poly(ethylene glycol) 400 (PEG, Sigma-Aldrich) and hexadecytrimethyl-ammonium bromide (HTAB, ≥ 98%) were used as surfactants (**Figures 1**–**4**).

2.2. Nanofluids preparation

Ultra sound sonication was used to homogenize the suspensions. The particles can be mixed into many different liquids at preferable concentrations. Probe-type sonicators break particle agglomerates faster and more thoroughly than bath sonicators, and thus, it was chosen for our experiments. The nanoparticles were dispersed mechanically in distilled water at a concentration of 0.05, 0.5, 1, 2 and 4% by volume for density and 0.05–0.5% by volume for viscosity.
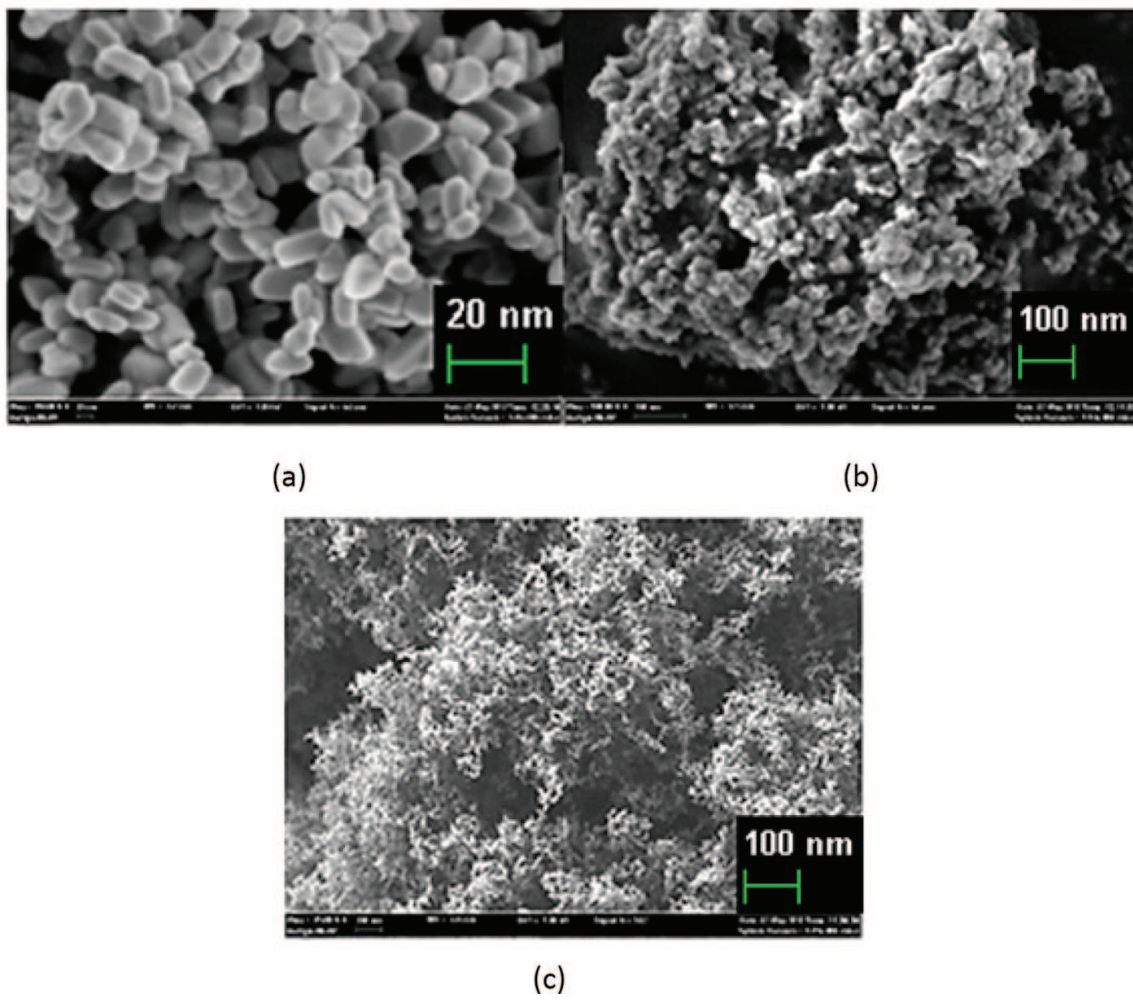
Figure 1. SEM images of (a) TiO$_2$, (b) SiO$_2$ and (c) Al$_2$O$_3$ nanoparticles.
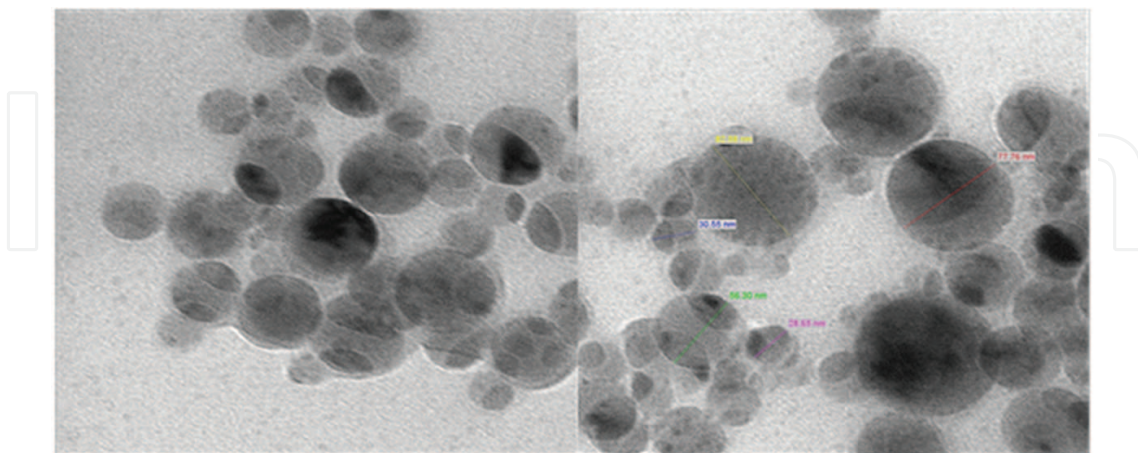

Figure 2. TEM images of silica (SiO$_2$) nanoparticles ~10 to 20 nm and with surfactant (0.14% PEG).

Aforementioned surfactants with 1:2, 1:3 and 1:5 nanoparticle to surfactant ratios (by volume) were used to prepare nanofluids for this research.
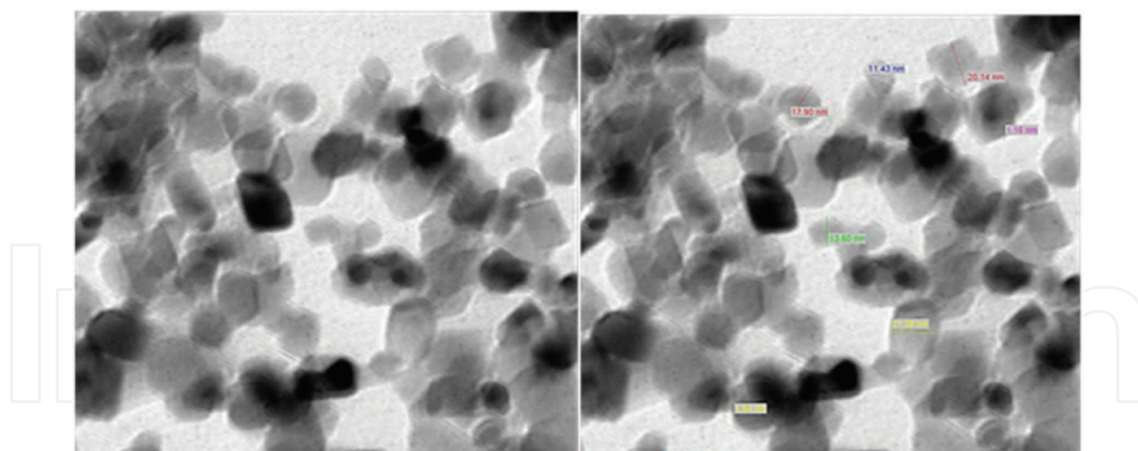
Figure 3. TEM images of titania (TiO$_2$) nanoparticles ~21 nm and the surfactant (0.1 %vol. PEG).
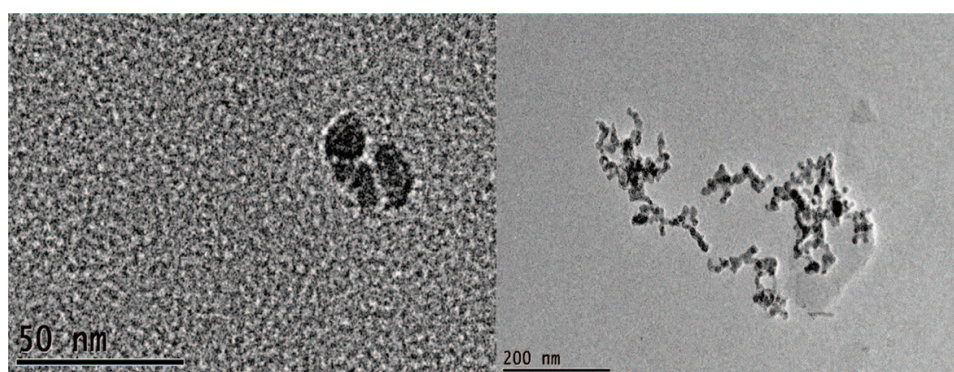

Figure 4. TEM images of alumina (Al$_2$O$_3$) nanoparticles, average 13 nm and the surfactant (0.1%vol. HTAB).

2.3. Nanofluid characterization

In order to characterize the prepared nanofluids, particle size, dynamic viscosity and density were measured as functions of temperature and particle volumetric fraction. Field emission scanning electron microscopy (FESEM) and transmission electron microscopy (TEM) were used to obtain the morphological characterization of the nanoparticles with SIGMA Zeiss instrument (Carl Zeiss SMT Ltd., UK). The Density Metre DA-130N from Kyoto Electronics Shinjuku-ku, Tokyo, Japan was used to measure the density of the nanofluids.

2.4. Sedimentation

Different nanofluids of 10 ml volume were used to investigate the sedimentation rate, and data were collected for 1 month from the date of preparation. **Table 1** shows the detailed description of our investigation. It was also found that 0.1 %vol. HTAB for TiO$_2$/DW and 0.1 %vol. PVP for Al$_2$O$_3$/DW and TiSiO$_4$/DW work as the best surfactants for stability.

From **Table 1**, it is noticed that all the nanoparticles, dispersed in DW, showed stability for longer periods of time, except for SiO$_2$.

Nanofluid	Surfactant	Sedimentation after 30 days (%)	Sedimentation rate (ml/day)
TiO$_2$/DW	0.1 %vol. PVP	95	0.317
	0.1 %vol. PEG	44	0.147
	0.15 %vol. PEG	42	0.140
	0.25 %vol. PEG	35	0.117
	0.1 %vol. HTAB	31	0.103
Al$_2$O$_3$/DW	0.1 %vol. PVP	10	0.033
	0.1 %vol. PEG	20	0.066
	0.15 %vol. PEG	27	0.090
	0.25 %vol. PEG	21	0.070
	0.1 %vol. HTAB	20	0.066
SiO$_2$/DW	0.1 %vol. PVP	99	9.9
	0.1 %vol. PEG	99	9.9
	0.15 %vol. PEG	99	9.9
	0.25 %vol. PEG	99	9.9
	0.1 %vol. HTAB	99	9.9

Table 1. Sedimentation rate of different nanofluids.

2.5. Density of nanofluid

Experimental data on density measurements are not sufficient for various nanofluids at varying temperatures in the literature. Therefore, we carried out comprehensive measurements to obtain density and provide data as well as to verify the applicability of Eq. (1) (which is also called as mixing theory) [15] for various nanofluids. **Figure 5** shows that density varies with temperature. Therefore, density equation should include temperature as a variable, whereas the mixing theory does not consider effect of temperature.

$$\rho_{nf} = \left(\frac{m}{V}\right)_{nf} = \frac{m_f + m_p}{V_f + V_p} = \frac{\rho_f V_f + \rho_p V_p}{V_f + V_p} = (1-\phi_p)\rho_{bf} + \phi_p\rho_p, \tag{1}$$

where $\phi_p = \frac{V_p}{V_f+V_p}$ is the volume fraction of the nanoparticles.

2.6. Theoretical models

In this section, the existing theoretical models and correlations for the viscosity of nanofluid suspensions are presented. Each model is used for specific circumstances.
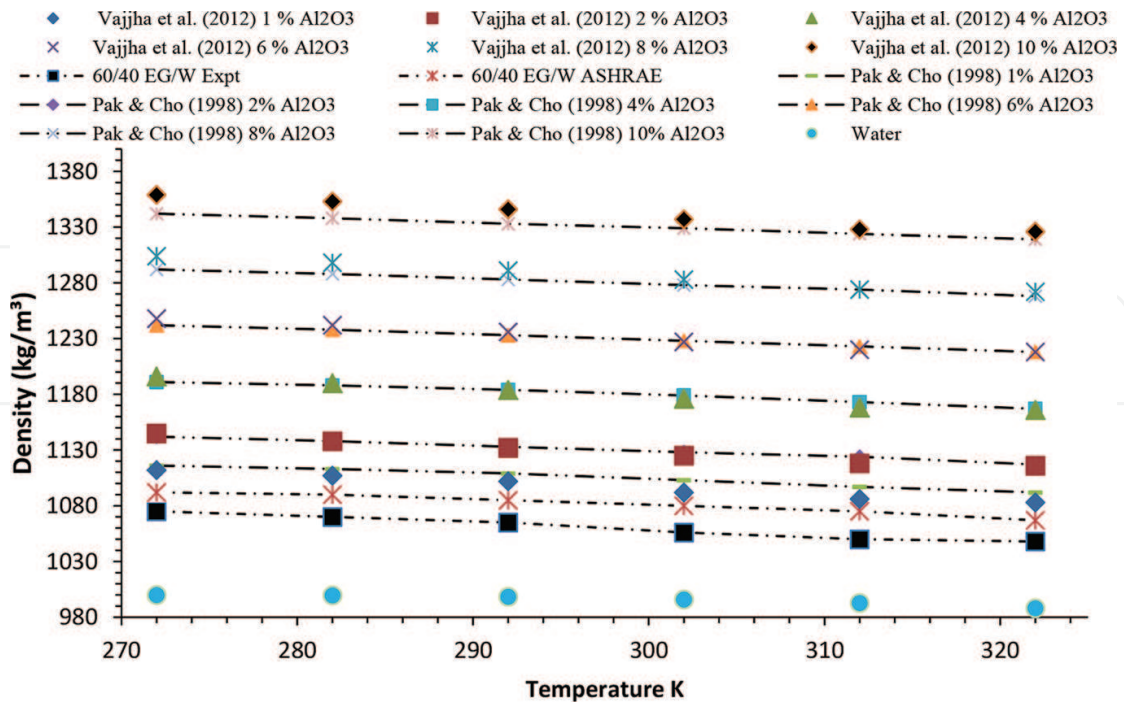
Figure 5. Densities of particle volumetric concentrations as a function of temperature [15, 27].

2.6.1. Implemented models for viscosity and density

In this part, the correlations that we have implemented for comparison between the experimental data and the predicted data are indicated.

$$\frac{\mu_{eff}}{\mu_f} = \frac{1}{1-34.87(d_p/d_f)^{-0.3}\varphi^{1.03}}, \quad where$$

$$d_f = 0.1\left(\frac{6M}{N\pi\rho_{bf}}\right)^{1/3}$$

(2)

It may be noted that once the base fluid is designated, the dimensionless effective viscosity of the nanofluid $\frac{\mu_{eff}}{\mu_f}$ increases with the decrease in particle diameter and increase in volume concentration.

2.6.2. Pumping power

The system counted is a forced flow nature. A pump is needed to mingle nanofluids throughout the system. The pump would require electrical energy. It is crucial to comprehend the entire energy needed by the pump to sustain a constant flow across the collector. The pumping power is analysed as follows [28]. The pressure drop throughout the collector is specified by Δp, which is determined from the subsequent equation [29]

$$\Delta p = f \frac{\rho V^2}{2} \frac{\Delta l}{d} + K \frac{\rho V^2}{2}, \tag{3}$$

where K is the loss coefficient because of entrance effects, exit effects, bends, elbows, valves, etc. V is the mean flow velocity of nanofluids in the system and is given by

$$V = \frac{\dot{m}}{\rho_{nf} \pi D_H^2 / 4}, \tag{4}$$

where D_H represents the hydraulic diameter. In present analysis consider D_H = pipe diameter (d). ρ_{nf} was calculated from Eq. (1). The frictional factor, f, for laminar and turbulent flow, correspondingly, is as follows [30]

$$f = \frac{64}{Re} \quad \text{for laminar flow}$$

$$f = \frac{0.079}{Re^{1/4}} \quad \text{for turbulent flow.}$$

The Reynolds number is composed as

$$Re = \frac{\rho V D_H}{\mu}. \tag{5}$$

Now, the pumping power can be calculated using Eq. (20)

$$\text{Pumping power} = \left(\frac{\dot{m}}{\rho_{nf}} \right) \Delta p. \tag{6}$$

2.6.3. Convective heat transfer

Elementary forced convective heat transfer model utters the interactions in the middle of fluid flow and convective heat transfer in terms of correlations between the dimensionless Reynolds, Prandtl and Nusselt numbers (Nu, Re and Pr, respectively). For the regular instances of laminar flows inside a pipe of diameter d, the theoretically developed relations are given as follows [31]:

$$h_{nf} = \frac{q}{T_W - T_f} \tag{7}$$

$$Nu_{nf} = \frac{h_{nf} d}{k_{nf}}. \tag{8}$$

The Nusselt number for the laminar flow throughout a circular pipe is the function of the Reynolds and Prandtl numbers and can be resolved by employing Eq. (8) [32]. Nusselt number,

Parameters of collector	Value
Type	Black paint flat plate
Glazing	Single glass
Agent fluids	Water, ethylene glycol and water mixture and Al_2O_3 nanofluids
Absorption area, A_p	1.51 m^2
Wind speed	20 m/s
Collector tilt, β_o	20°
Ambient temperature, T_a	300 K
Apparent sun temperature, T_s	4350 K
Optical efficiency, η_o	0.84
Glass thickness, t	4 mm
Insulation thermal conductivity, k_i	0.06 W/mK
Incident solar energy per unit area of the absorber plate, I_T	1000 W/m^2
Inner diameter of pipes, d	0.01 m

Table 2. Environmental and analysis conditions for the flat plate solar collector.

$$Nu = 0.000972 Re^{1.17} Pr^{1/3} \text{ for Re} < 2000, \tag{9}$$

where Pr and k_{nf} can be expressed as,

$$Pr = \frac{C_{p,nf}\,\mu_{nf}}{k_{nf}} \tag{10}$$

$$\frac{k_{nf}}{k_f} = \frac{k_p + (SH-1)k_f - (SH-1)\varphi(k_f - k_p)}{k_p + (SH-1)k_f + \varphi(k_f - k_p)}. \tag{11}$$

In Eq. (12), SH is the shape factor, which is given to be three for the spherical shape of nanoparticle [33] (**Table 2**).

3. Results and discussions

3.1. Size distribution of the nanoparticles

SEM nano-graphs of (a) TiO_2, (b) SiO_2 and (c) Al_2O_3 nanoparticles are presented in **Figure 1**. **Figure 2** presents the TEM images of silica (SiO_2) nanoparticles with surfactant (0.14% PEG). **Figure 3** presents the TEM images of titania (TiO_2) nanoparticles ~21 nm and the surfactant (0.1 %vol. PEG). **Figure 4** presents the TEM images of alumina (Al_2O_3) nanoparticles, average 13 nm and the surfactant (0.1%vol. HTAB).
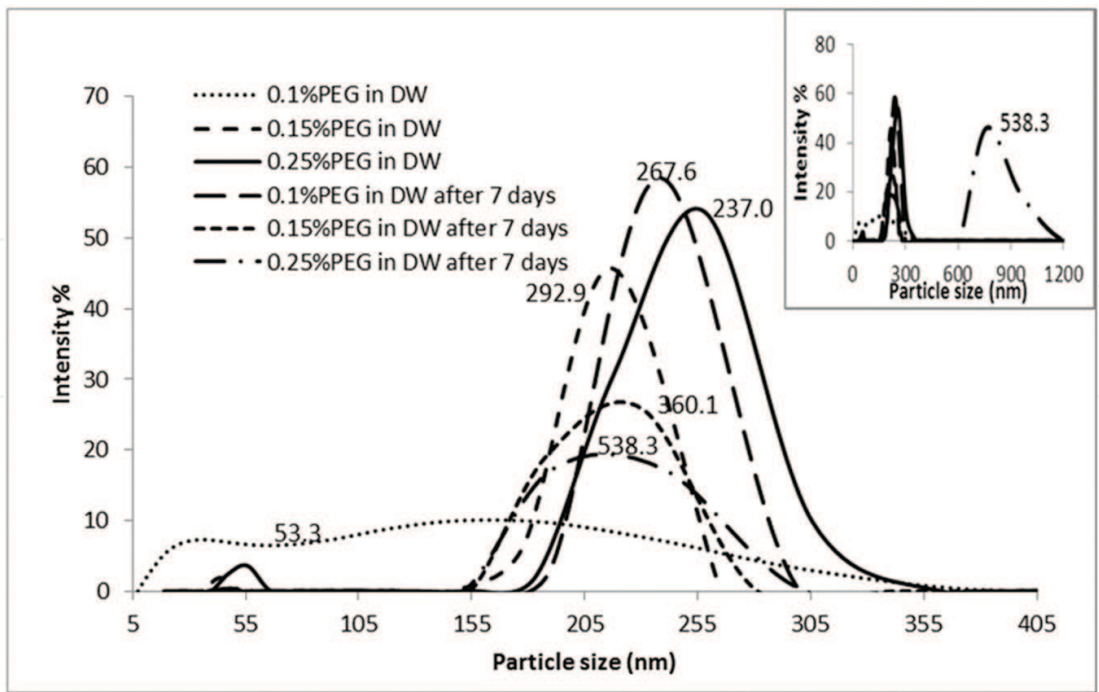
Figure 6. Size distribution of the nanoparticles in 0.05 %vol. water-based TiO$_2$ nanofluids with surfactants. Inset is the full size distribution.
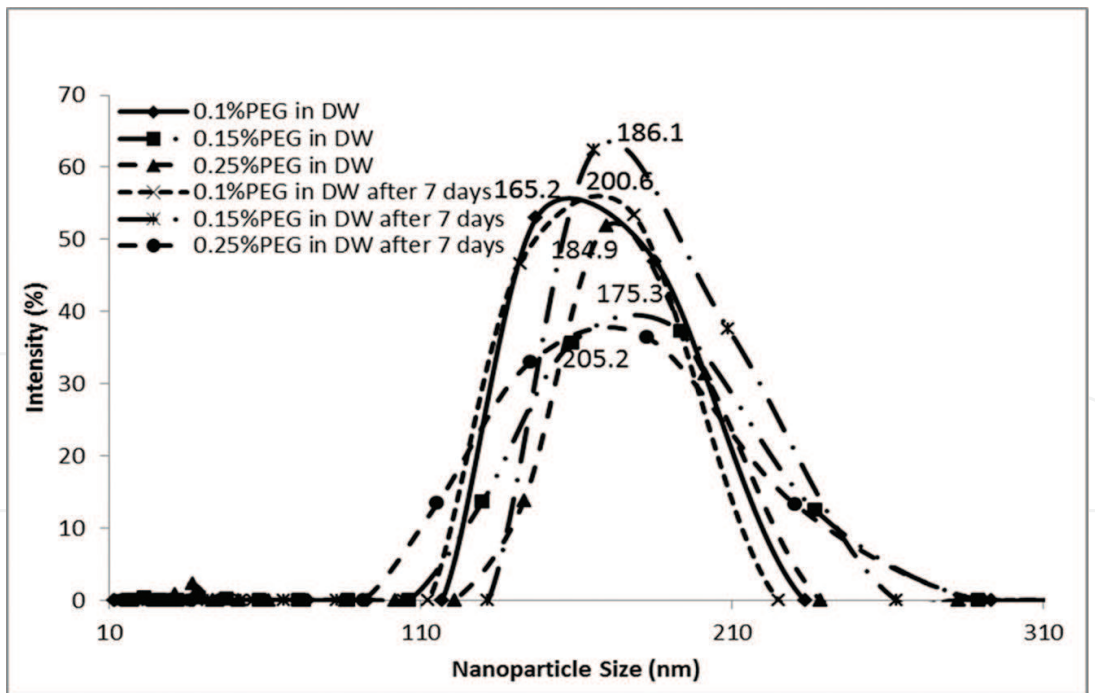
Figure 7. Size distribution of the nanoparticles in 0.05 %vol. water-based Al$_2$O$_3$ nanofluids with surfactants.

Sizes of the nanoparticles in all the prepared nanofluids were measured using Zetasizer3000HSa (Malvern), and results for the most stable nanofluids are shown in **Figures 6** and **7**.

The numbers placed at the apexes describe the average particle size as obtained from the machine. It should be noted that the Malvern Nanosizer measures hydrodynamic properties based on the Strokes-Einstein equation, which is expected to be slightly larger than the actual size. Incorporating the findings from those in **Figures 6** and **7**, it is found that the visual sedimentation rate of TiO$_2$/water nanofluid decreases with increasing surfactant (PEG), whereas particle size increases with the increase in surfactant. For Al$_2$O$_3$/water nanofluid, the sedimentation rate for PEG in different concentrations is approximately similar and the size distribution of the particles is approximately also in the same region. The stability of the stable nanofluids as shown in **Figures 6** and **7** was obtained for more than 1 week.

3.2. Density of nanofluids

First, a benchmark test for the density of the base fluid is presented showing excellent agreement with the data presented in the handbook of the American Society of Heating, Refrigerating and Air-Conditioning Engineers (ASHRAE). Next, density measurements of the TiO$_2$, Al$_2$O$_3$ and SiO$_2$ nanofluids over a temperature range of 25–40°C for several particle volume concentrations are presented. These measured results were compared with a widely used theoretical equation, and good agreements between the theoretical equation and measurements were obtained for the TiO$_2$, Al$_2$O$_3$ and SiO$_2$ nanofluids.

We found the density decreasing with the increase in temperature. Eq. (1) is used to make the comparison with our experimental data. **Figures 8** and **9** show the experimental values at different temperatures and the theoretical value obtained from Pak and Cho [15]. The trend lines generated from the experimental values clearly certify the linear relationship of density with concentration at a particular temperature. It also validates that the density increases with the increase in concentration. The pattern of the change in density is analysed, and the
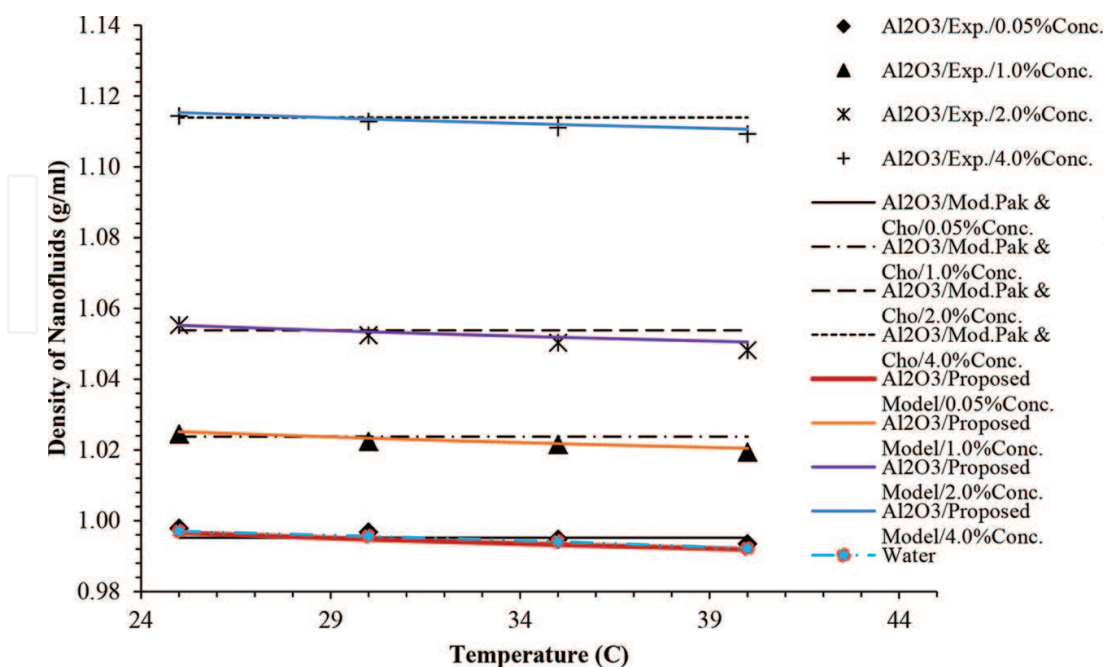

Figure 8. Density vs. temperature graph of Al$_2$O$_3$–water nanofluid at different concentrations.
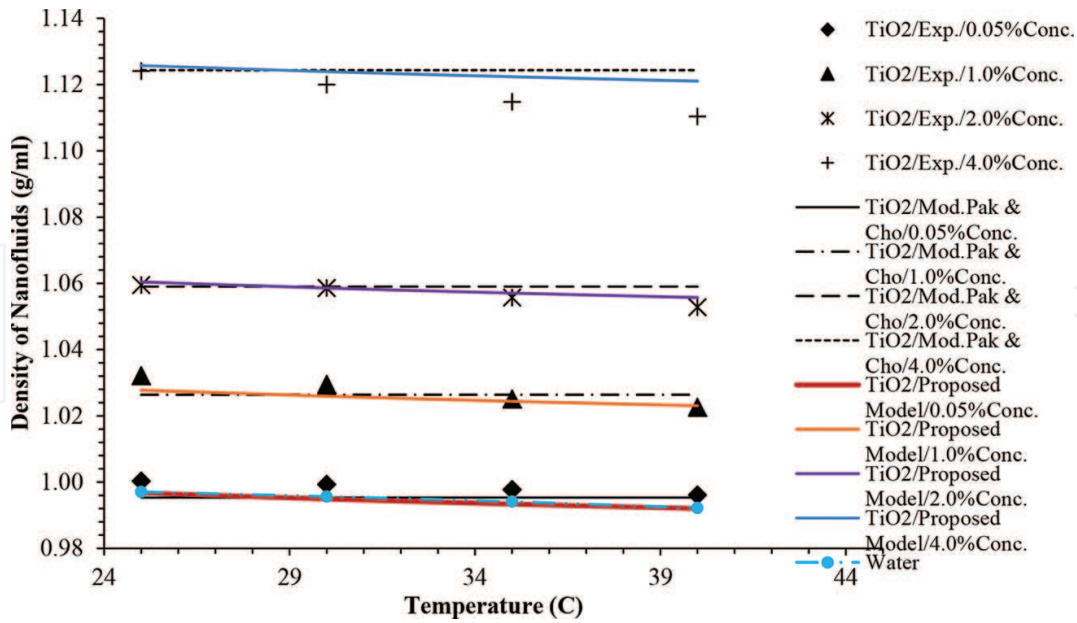
Figure 9. Density vs. temperature graph of TiO$_2$–water nanofluid at different concentrations.

proposed empirical formula is presented below. The effective density of the nanofluids is measured using authors' proposed formula derived based on Einstein's theory. This model considers the changing temperature, volume fraction as well as the size of the nanoparticles. No such models have been presented previously, which also justifies the novelty of this proposed formula.

$$\rho_{nf} = (1-\phi_p)\rho_{bf} + \phi_p\rho_p + \left(a - \frac{\ln(T)}{100}\right), \text{where } a = 0.03358. \tag{12}$$

Moreover, as we examine the average absolute percentage deviation, we notice a systematic increase in percentage deviation with the concentration, as shown in **Figures 8–10**. Further examination shows a gradual increase in percentage deviation with the temperature. There-fore, the proposed equation may have limitations for some nanofluids. The proposed formula is found valid for up to 2 %vol. concentration. The maximum relative difference between the experimental and theoretical values is 0.3% for Al$_2$O$_3$, 0.44% for TiO$_2$ and 0.28% for SiO$_2$. **Figures 8–10** represent the comparative graph for experimental data, Pak and Cho model data and proposed model data (solid line).

3.3. Viscosity

Viscosity of water-based nanofluids with and without surfactant was experimentally obtained. Viscosity of nanofluid was measured using Brookfield viscometer (DV-II + Pro Programmable Viscometer), which was connected with a temperature controlled bath. To verify the accuracy of our equipment and experimental procedure, viscosity of the ethylene glycol and water mixture (60:40 by mass) was measured and compared with the data from the American Society of Heating, Refrigerating and Air-Conditioning Engineers (ASHRAE) handbook [34].
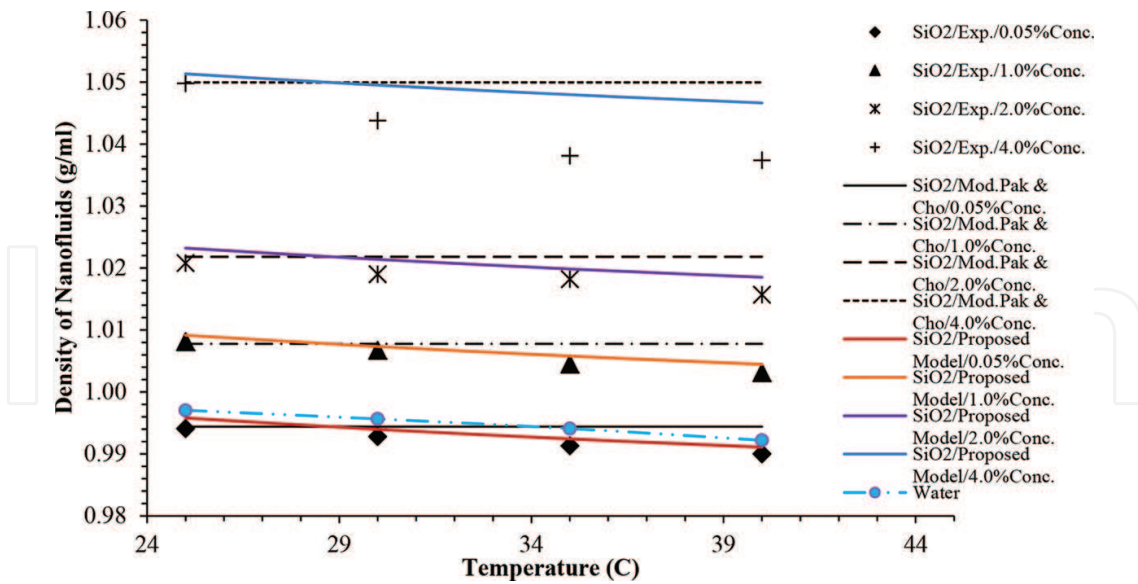
Figure 10. Density vs. temperature graph of SiO$_2$–water nanofluid at different concentrations.
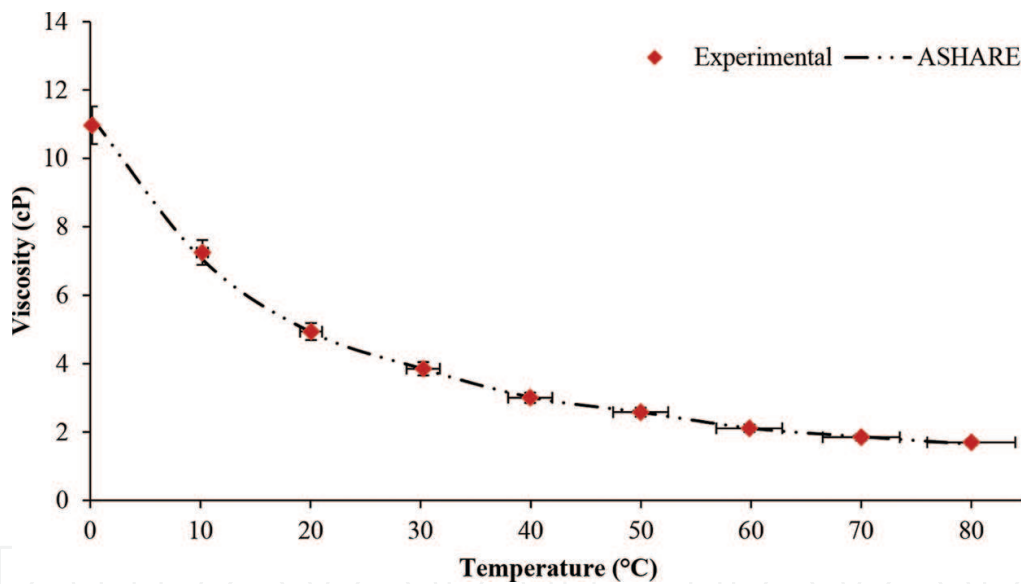

Figure 11. Comparison of ASHRAE viscosity values of 60:40 ethylene glycol and water mixture (by mass) and experimental data. 1 cP (centipoise) = 1 mPa s.

Before conducting the density measurement, the equipment must be calibrated. Density measurements of a mixture of 60:40 EG/W by mass were first conducted to confirm the accuracy of our apparatus and the calibration procedure. The results of these measurements and the data from ASHRAE are presented in **Figure 11** over a temperature range of 0–80°C. Excellent agreement is observed between the current measurements and the ASHRAE data. **Figure 11** shows that the experimental values of viscosity for the ethylene glycol mixture and the ASHRAE data match fairly with a maximum alteration of ±2.0%. The deviations at low shear rates were due to machine error.
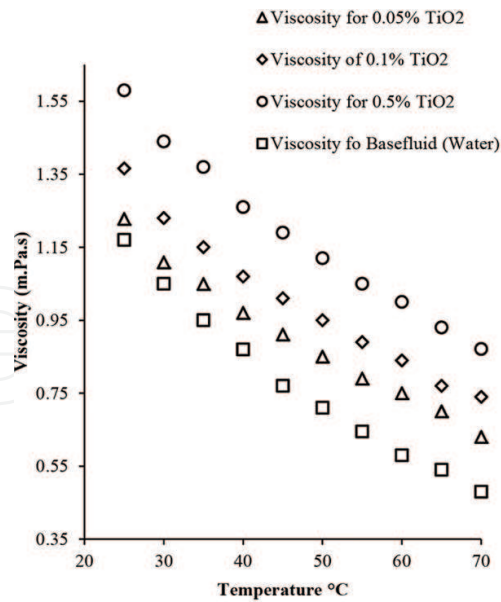
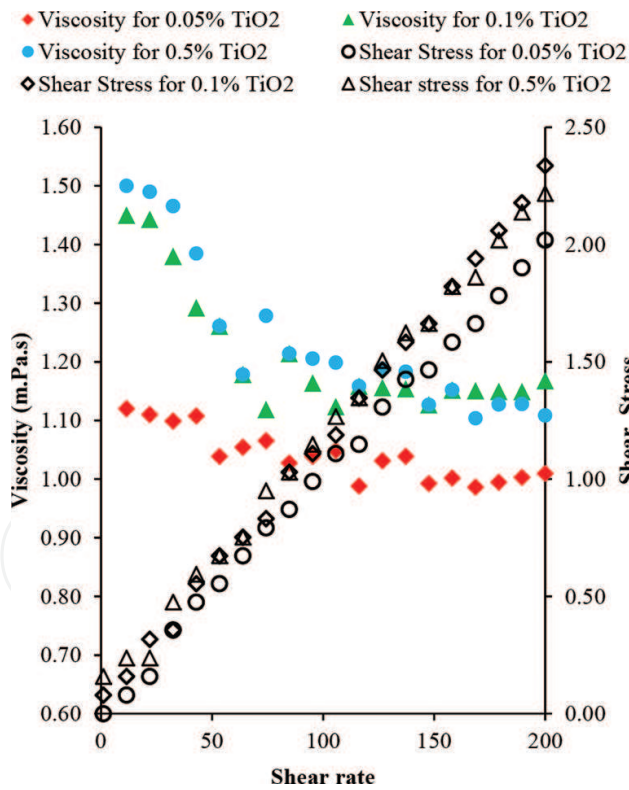**Figure 12.** Viscosity of TiO_2 at different temperatures and concentrations.

Figure 13. Viscosity of TiO_2 at different shear rates and concentrations.

Viscosity of TiO_2-H_2O with different volume concentration and changing temperature is presented in **Figure 12**. It is observed that the viscosity reduces with the increase in temperature and rises with the increase in volume fraction. From **Figure 13** at 0.5 vol.%, titanium
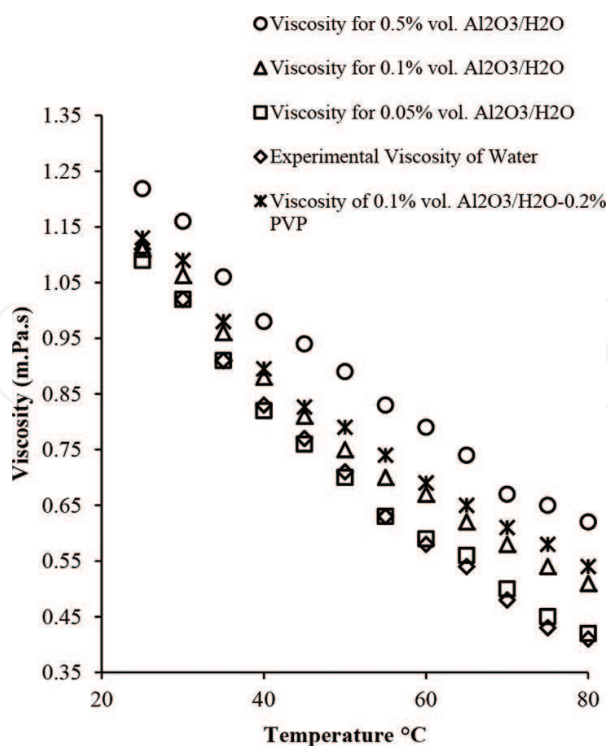
Figure 14. Viscosity of Al_2O_3 at different temperatures and concentrations.

behaves in a non-Newtonian way after 40°C. For the whole temperature range, this nanofluid demonstrates a Newtonian behaviour at 0.05 vol.%, while a non-Newtonian nature is found for 0.1 vol.%.

From **Figure 14**, the effect of surfactant is observed to increase viscosity. Addition of surfactant augments the viscosity of the nanofluid. Similarly, viscosity tends to increase in **Figure 15**, for alumina with the rise in the volume concentration as well as addition of surfactants. As opposed to thermal conductivity, viscosity of these nanofluids showed a decreasing trend with the increase in temperature. Furthermore, a nonlinear relation is observed between the viscosity of alumina nanofluid and particle concentration except for 0.05 vol.% and temperatures lower than 40°C.

As it is observed from **Figure 15**, in the case of nanoparticles with surfactants, viscosity tends to decrease due to augmenting the temperature. This can be explained by the change in the shape of micelles. Worm shapes change to spherical or vesicles which lead to the destruction of network structure and consequently a decrease in viscosity through temperature rise [35]. After the breakdown in network occurs, the attractive forces between the particles become dominant to produce aggregates.

Viscosity of SiO_2 at different temperatures and concentrations is illustrated in **Figure 16**. It is witnessed that the rise in temperature results in reduced viscosity and addition of volume fraction also results in higher viscosity. **Figure 17** presents the changes in the viscosity for SiO_2 nanofluid. In this case, the viscosity keeps increasing up to the concentration of 0.1 vol.%, but remains unchanged afterwards. This is because SiO_2 nanofluid is not stable, and due to the high rate of aggregation, sedimentation of nanoparticles takes place and consequently no
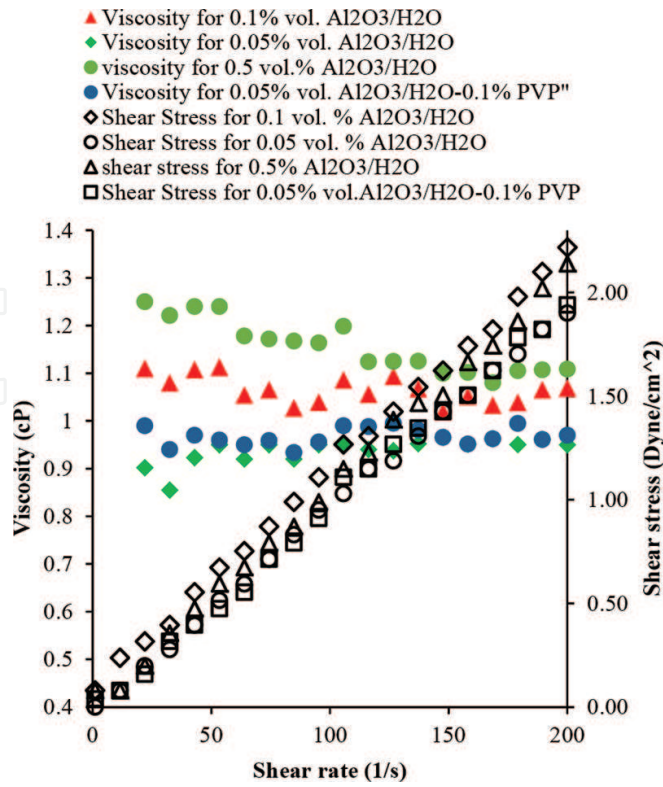
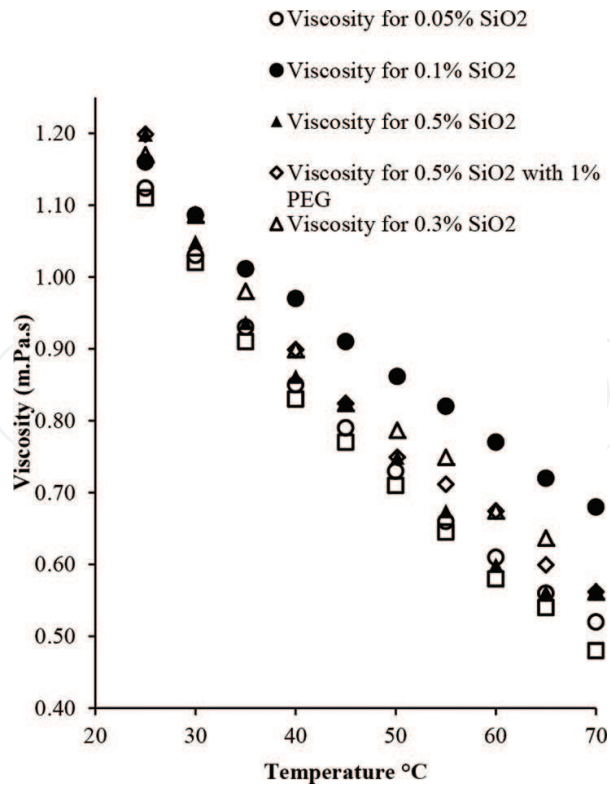**Figure 15.** Viscosity of Al_2O_3 at different shear rate and concentrations.

Figure 16. Viscosity of SiO_2 at different temperatures and concentrations.
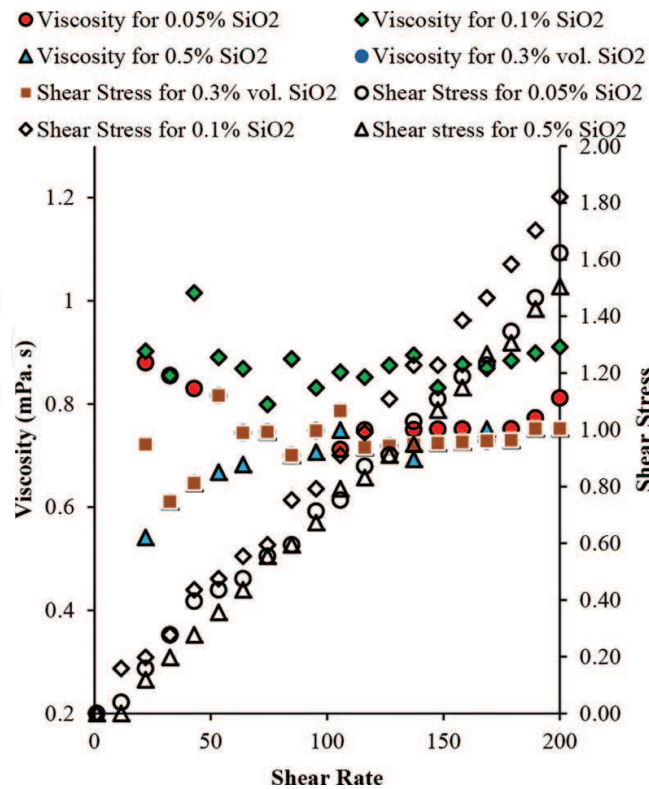
Figure 17. Viscosity of SiO_2 at different shear rate and concentrations.

increment is observed. Adding surfactant causes minor increments in the viscosity of the nanofluid, with no significant changes in the stability of the colloid even after a period of half an hour. Newtonian behaviour is found for this nanofluid at 0.05 vol.% for temperatures over 50°C, but non-Newtonian characteristics are shown beyond this point. A similar trend occurred for 0.5 vol.% and at 60°C. A non-Newtonian behaviour for the entire range of temperature is observed for 0.1 vol.%.

In the previous articles, it was claimed that the viscosity of nanofluids is mainly dependent on the concentration of nanoparticles, properties of base fluid and temperature. However, some also reported about the size of the nanoparticles. From the results of current study, it is observed that for the same concentration (0.5%vol.), viscosities of the nanofluids are different, and TiO_2 results in higher viscosity followed by Al_2O_3 and SiO_2 nanofluids for 0.5 vol.% concentration. Therefore, it can be said that viscosity depends on nanoparticles' properties such as the size and density. The available models are not appropriate to forecast or measure accurate viscosity of nanofluids as they are not related to temperature variation and nanoparticles' properties. Therefore, the results suggest the requirement of providing a more generalized viscosity model.

3.4. Pumping power and convective heat transfer

The resulting pressure losses are analysed in detail in this section. **Figure 18** presents the pumping power and pressure drop with respect to volume fraction and volume flow rate for
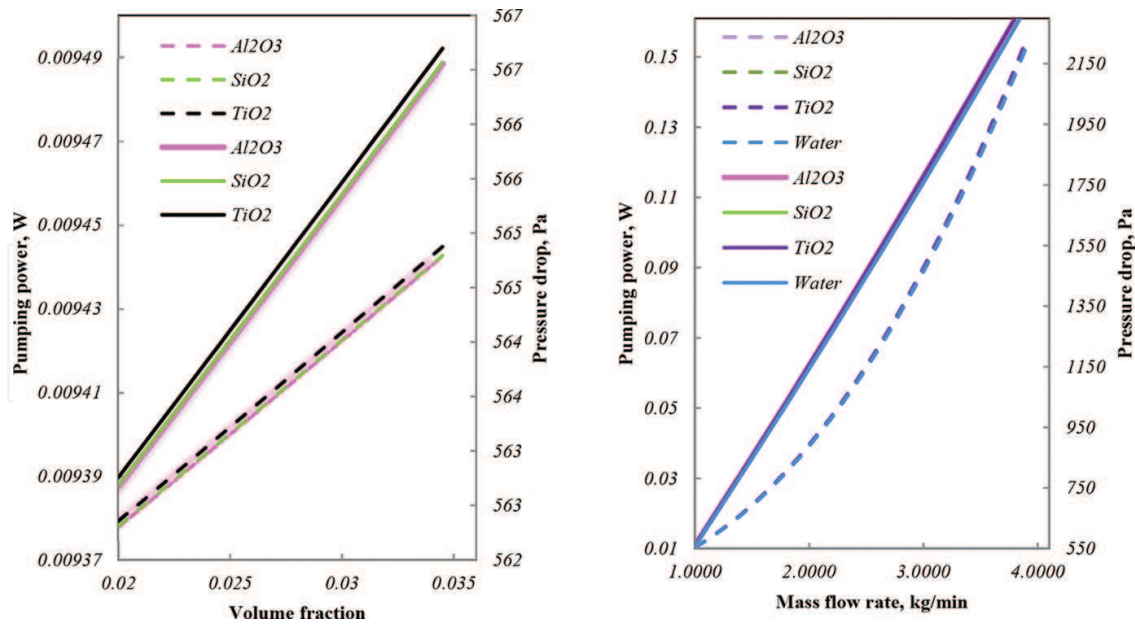
Figure 18. Effect of volume fraction and mass flow rate on pumping power (solid line) and pressure drop (dotted line).

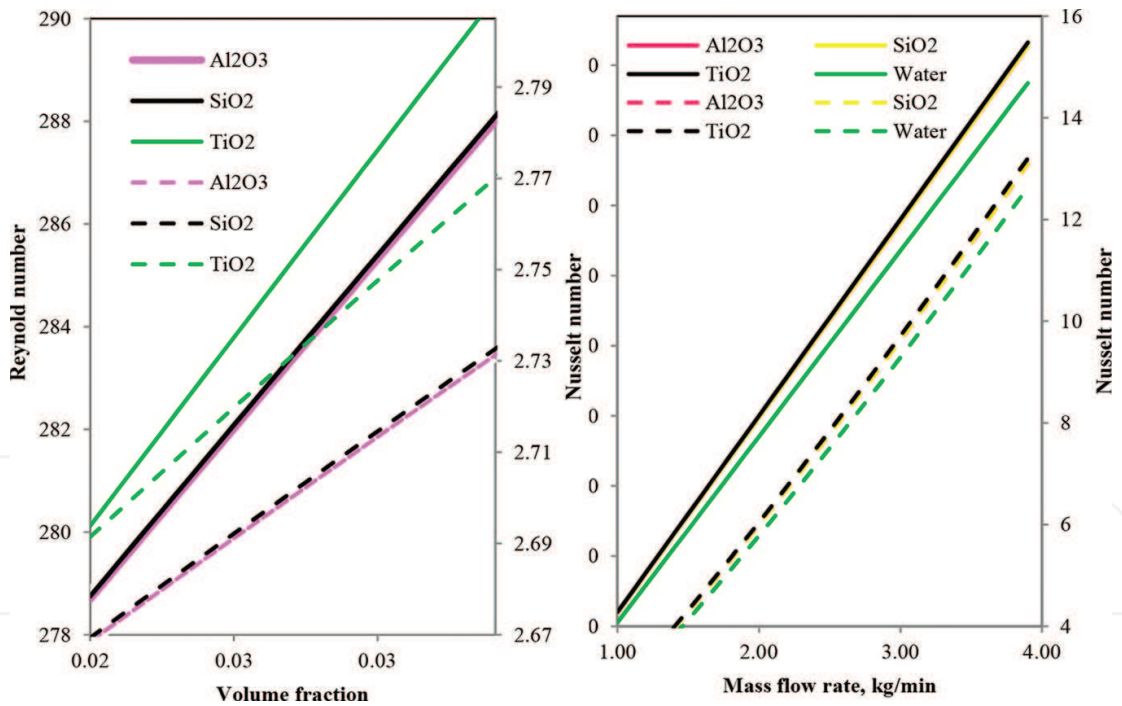**Figure 19.** Effect of volume fraction and mass flow rate on the Reynolds number and Nusselt number.

the laminar flow, respectively. These two parameters are calculated using Eqs. (4) to (7) and **Table 1**.

The results show that the friction factor enhances with the increase in volume fraction and flow rate. It is observed from the figures that the friction factors of the nanofluids are almost the

same as that of the base fluid under same nanoparticle volume concentrations, therefore resulting in little supplementary pumping power for the process [36–38].

Effect of volume fraction and mass flow rate is presented in **Figure 19**. These parameters are calculated using Eqs. (6) and (9). With the rising volume fraction of the nanoparticles suspended in water, it is observed that the both the Reynolds number and Nusselt number increase slightly in comparison with water. Reynolds number and Nusselt numbers of the nanofluid are greater compared to water, and the numbers are rising with the growing volume fraction as well as with the rising mass flow rate. This shows that increasing the molecular thermal diffusion due to increasing the nanoparticles volume fraction is the foremost purpose of the heat transfer enhancement for an exact Reynolds number. As a significance, the increase in the Nusselt number is found with a rise in Re. An alike trend was also witnessed by Maïga et al. [39].

The experimental results clearly show that the nanoparticles suspended in water enhance the convective heat transfer coefficient, although the volume fraction of nanoparticles is very low ranging from 0.01 to 0.3 vol.%. The convective heat transfer coefficient of water-based Al_2O_3 nanofluids increases with volume fraction of Al_2O_3 nanoparticles as shown in **Figure 20**.

The overall heat transfer coefficient of water rises with the rising mass flow rate, with a maximum value of 804 W/m^2 compared to that of water, which is 732 W/m^{2}K with the highest flow rate investigated. Heat transfer coefficient is improved with the addition of volume fraction as well as with the mass flow rate. Heat transfer coefficient is directly proportional to heat rate.

From the above results presented in the figures, it can be concluded that the heat transfer coefficient enhanced up to 15% with the suspended nanoparticles in the base fluid. The
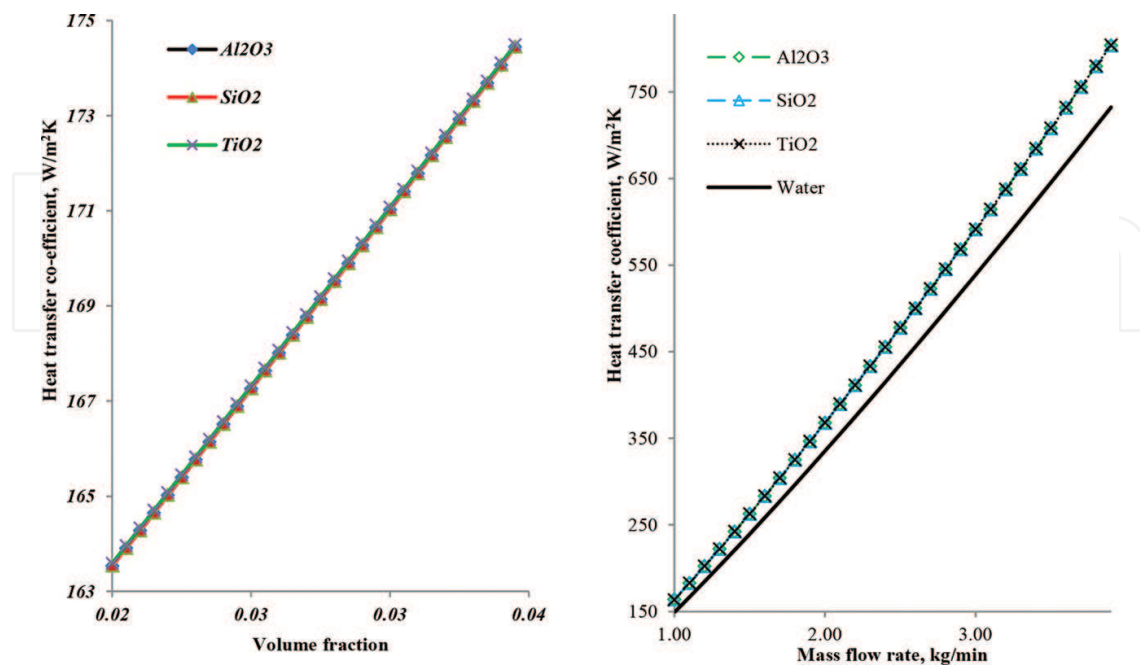

Figure 20. Heat transfer coefficient with respect to changing volume fraction and mass flow rate.

patterns shown by the oxide nanofluids are due to the fact that the addition of nanoparticles tends to enhance the thermal conductivity, density and viscosity of the base fluid. The enhancement in Reynolds number and Nusselt number was observed to be 8.4, 7.6 and 7.5% for TiO_2, SiO_2 and Al_2O_3, respectively. Nusselt number was improved by 6.8, 5.5 and 5.4%, for TiO_2, SiO_2 and Al_2O_3, respectively. This enhancement results in heat transfer performance. Enhancement in pumping power was observed to be 1.5%.

4. Future recommendations

The prospect of using nanofluids in different applications is related to their thermal and flow properties. Measurement of these properties will be performed in near future in order to access the total improvement in energy efficiency where these fluids are being used. Despite some undesirable changes such as rising viscosity or decreasing specific heat, we can consider nanofluids as good thermal fluids. However, researches to obtain a comprehensive formula to determine other physical properties of nanofluid must be continued.

5. Conclusion

The effect of volume fraction, temperature and mass flow rate was investigated on density, viscosity, pumping power and convective heat transfer of nanofluids in this article. Stability of nanofluids was obtained using different surfactants. Important conclusions have been attained and summarized as follows:

1. The density is found decreasing with the increase in temperature. An empirical model is proposed to describe the behaviour. The maximum deviation between the experimental values and the proposed model is 0.3% for Al_2O_3, 0.44% for TiO_2 and 0.3% for SiO_2 which is very small and well below the minimum acceptable limit (1%).

2. Viscosity of our nanofluids increases dramatically with the increase in particle concentration. Addition of surfactants results in part of the increment.

3. Friction factor rises with the rising volume fraction. This is due to the increasing density and viscosity with the addition of nanoparticles. Since this effect is slightly higher compared to base fluid, therefore little penalty in pressure drop and pumping power occurs.

4. At a particle volume concentration of 3%, the use of oxide nanofluid gives significantly higher heat transfer characteristics. For example, at the particle volume concentration of 3%, the overall heat transfer coefficient is 804 W/m^2 compared to that of water, which is 732 W/m^2 for a mass flow rate of 1 kg/min, so the overall heat transfer coefficient of the oxides nanofluid is 15% greater than that of distilled water as a base fluid.

5. The enhancement in Reynolds number Nusselt number was observed to be 8.4, 7.6 and 7.5% for TiO_2, SiO_2 and Al_2O_3, respectively. Nusselt number was improved by 6.8, 5.5

and 5.4%, for TiO_2, SiO_2 and Al_2O_3, respectively, which is greater than that of distilled water.

Acknowledgements

Nomenclature

d	diameter
f	friction factor
FESEM	field emission scanning electron microscopy
k	thermal conductivity, W/mK
Re	Reynolds number
SEM	scanning electron microscopy
T	temperature, °C
TEM	transmission electron microscopy
Δp	pressure drop, Pa

Greek symbols

ρ	density, kg m^{-3}
ϕ	volumetric fraction
μ	volumetric fraction
η	intrinsic viscosity
δ	thickness of nano-layer

Subscripts

bf	base fluid
nf	nanofluid
p	particle

Author details

Zafar Said[1,2]* and Rahman Saidur[2,3]

*Address all correspondence to: zaffar.ks@gmail.com; zsaid@masdar.ac.ae

1 Department of Sustainable and Renewable Energy Engineering (SREE), University of Sharjah, Sharjah, United Arab Emirates

2 Department of Mechanical Engineering, Faculty of Engineering, University of Malaya, Kuala Lumpur, Malaysia

3 Centre of Research Excellence in Renewable Energy (CoRE-RE), King Fahd University of Petroleum and Minerals (KFUPM), Dhahran, Saudi Arabia

References

[1] Eastman, J., S. Choi, S. Li, W. Yu, and L. Thompson, Anomalously increased effective thermal conductivities of ethylene glycol-based nanofluids containing copper nanoparticles. Applied Physics Letters. **78**(6)(2001): p. 718–720.

[2] Das, S.K., N. Putra, P. Thiesen, and W. Roetzel, Temperature dependence of thermal conductivity enhancement for nanofluids. Journal of Heat Transfer. **125**(2003): p. 567.

[3] Xuan, Y. and Q. Li, Investigation on convective heat transfer and flow features of nanofluids. Journal of Heat Transfer. **125**(2003): p. 151.

[4] Reddy, M., V.V. Rao, B. Reddy, S.N. Sarada, and L. Ramesh, Thermal conductivity measurements of ethylene glycol water based TiO_2 nanofluids. Nanoscience and Nanotechnology Letters. **4**(1)(2012): p. 105–109.

[5] Wamkam, C.T., M.K. Opoku, H. Hong, and P. Smith, Effects of ph on heat transfer nanofluids containing ZrO_2 and TiO_2 nanoparticles. Journal of Applied Physics. **109** (2011): p. 024305.

[6] Xie, H., W. Yu, and W. Chen, Mgo nanofluids: higher thermal conductivity and lower viscosity among ethylene glycol-based nanofluids containing oxide nanoparticles. Journal of Experimental Nanoscience. **5**(5)(2010): p. 463–472.

[7] Turgut, A., I. Tavman, M. Chirtoc, H. Schuchmann, C. Sauter, and S. Tavman, Thermal conductivity and viscosity measurements of water-based TiO_2 nanofluids. International Journal of Thermophysics. **30**(4)(2009): p. 1213–1226.

[8] Li, Y., J.e. Zhou, S. Tung, E. Schneider, and S. Xi, A review on development of nanofluid preparation and characterization. Powder Technology. **196**(2)(2009): p. 89–101.

[9] Duangthongsuk, W. and S. Wongwises, Measurement of temperature-dependent thermal conductivity and viscosity of TiO_2-water nanofluids. Experimental Thermal and Fluid Science. **33**(4)(2009): p. 706–714.

[10] Ghadimi, A., R. Saidur, and H. Metselaar, A review of nanofluid stability properties and characterization in stationary conditions. International Journal of Heat and Mass Transfer. **54**(17)(2011): p. 4051–4068.

[11] Ramesh, G. and N.K. Prabhu, Review of thermophysical properties, wetting and heat transfer characteristics of nanofluids and their applicability in industrial quench heat treatment. Nanoscale Research Letters. **6**(1)(2011): p. 1–15.

[12] Trisaksri, V. and S. Wongwises, Critical review of heat transfer characteristics of nanofluids. Renewable and Sustainable Energy Reviews. **11**(3)(2007): p. 512–523.

[13] Timofeeva EV, Yu W, France DM, Singh D, Routbort JL. Nanofluids for heat transfer: an engineering approach. Nanoscale research letters. 2011 Feb 28;6(1):1.

[14] Cheremisinoff, N. P. "Encyclopedia of fluid mechanics. Volume 1-Flow phenomena and measurement." Encyclopedia of Fluid Mechanics. Volume 1. Vol. 1. 1986.

[15] Pak, B.C. and Y.I. Cho, Hydrodynamic and heat transfer study of dispersed fluids with submicron metallic oxide particles. Experimental Heat Transfer an International Journal. **11**(2)(1998): p. 151–170.

[16] Bobbo, S., L. Fedele, A. Benetti, L. Colla, M. Fabrizio, C. Pagura, and S. Barison, Viscosity of water based swcnh and TiO_2 nanofluids. Experimental Thermal and Fluid Science. **36** (2012): p. 65–71.

[17] Chandrasekar, M., S. Suresh, and A. Chandra Bose, Experimental investigations and theoretical determination of thermal conductivity and viscosity of Al_2O_3 water nanofluid. Experimental Thermal and Fluid Science. **34**(2)(2010): p. 210–216.

[18] Chen, H., Y. Ding, Y. He, and C. Tan, Rheological behaviour of ethylene glycol based titania nanofluids. Chemical Physics Letters. **444**(4)(2007): p. 333–337.

[19] Fedele, L., L. Colla, and S. Bobbo, Viscosity and thermal conductivity measurements of water-based nanofluids containing titanium oxide nanoparticles. International Journal of Refrigeration. **35**(5)(2012): p. 1359–1366.

[20] Timofeeva, E.V., A.N. Gavrilov, J.M. McCloskey, Y.V. Tolmachev, S. Sprunt, L.M. Lopatina, and J.V. Selinger, Thermal conductivity and particle agglomeration in alumina nanofluids: experiment and theory. Physical Review E. **76**(6)(2007): p. 061203.

[21] Pastoriza-Gallego, M., C. Casanova, J. Legido, and M. Piñeiro, Cuo in water nanofluid: influence of particle size and polydispersity on volumetric behaviour and viscosity. Fluid Phase Equilibria. **300**(1)(2011): p. 188–196.

[22] Koo, J., Computational nanofluid flow and heat transfer analyses applied to micro-systems. (2005).

[23] Masoumi, N., N. Sohrabi, and A. Behzadmehr, A new model for calculating the effective viscosity of nanofluids. Journal of Physics D: Applied Physics. **42**(5)(2009): p. 055501.

[24] Meriläinen, A., A. Seppälä, K. Saari, J. Seitsonen, J. Ruokolainen, S. Puisto, N. Rostedt, and T. Ala-Nissila, Influence of particle size and shape on turbulent heat transfer characteristics and pressure losses in water-based nanofluids. International Journal of Heat and Mass Transfer. **61**(2013): p. 439–448.

[25] Sheikholeslami, M. and D. Ganji, Heat transfer of Cu-water nanofluid flow between parallel plates. Powder Technology. **235**(2013): p. 873–879.

[26] Sheikholeslami, M. and D.D. Ganji, Unsteady nanofluid flow and heat transfer in presence of magnetic field considering thermal radiation. Journal of the Brazilian Society of Mechanical Sciences and Engineering. **37**(3)(2015): p. 895–902.

[27] Vajjha, R.S. and D.K. Das, A review and analysis on influence of temperature and concentration of nanofluids on thermophysical properties, heat transfer and pumping power. International Journal of Heat and Mass Transfer. **55**(15)(2012): p. 4063–4078.

[28] Garg, H.P. and R.K. Agarwal, Some aspects of a pv/t collector/forced circulation flat plate solar water heater with solar cells. Energy Conversion and Management. **36**(2)(1995): p. 87–99.

[29] White, F.M., Fluid mechanics. 5th edition. Boston: McGraw-Hill Book Company. (2003).

[30] Kahani, M., S. Zeinali Heris, and S. M. Mousavi. "Effects of curvature ratio and coil pitch spacing on heat transfer performance of Al2O3/water nanofluid laminar flow through helical coils." Journal of Dispersion Science and Technology 34.12 (2013): 1704-1712

[31] Li, Q., Y. Xuan, and J. Wang, Investigation on convective heat transfer and flow features of nanofluids. Journal of Heat Transfer. **125**(2003): p. 151–155.

[32] Owhaib, W. and B. Palm, Experimental investigation of single-phase convective heat transfer in circular microchannels. Experimental Thermal and Fluid Science. **28**(2)(2004): p. 105–110.

[33] Li, Feng-Chen, et al. "Experimental study on the characteristics of thermal conductivity and shear viscosity of viscoelastic-fluid-based nanofluids containing multiwalled carbon nanotubes." Thermochimica Acta 556 (2013): 47-53.

[34] Handbook, A., 1985 Fundamentals. American Society of Heating, Refrigerating, and Air Conditioning Engineers, Inc., Atlanta, Georgia. (1985).

[35] Mingzheng, Z., X. Guodong, L. Jian, C. Lei, and Z. Lijun, Analysis of factors influencing thermal conductivity and viscosity in different kinds of surfactant solutions. Experimental Thermal and Fluid Science. **36**(2012): p. 22–29.

[36] Mahian, O., A. Kianifar, S.A. Kalogirou, I. Pop, and S. Wongwises, A review of the applications of nanofluids in solar energy. International Journal of Heat and Mass Transfer. **57**(2)(2013): p. 582–594.

[37] Gherasim, I., G. Roy, C.T. Nguyen, and D. Vo-Ngoc, Heat transfer enhancement and pumping power in confined radial flows using nanoparticle suspensions (nanofluids). International Journal of Thermal Sciences. **50**(3)(2011): p. 369–377.

[38] Hwang, K.S., S.P. Jang, and S.U. Choi, Flow and convective heat transfer characteristics of water-based Al_2O_3 nanofluids in fully developed laminar flow regime. International Journal of Heat and Mass Transfer. **52**(1)(2009): p. 193–199.

[39] Maïga, S.E.B., S.J. Palm, C.T. Nguyen, G. Roy, and N. Galanis, Heat transfer enhancement by using nanofluids in forced convection flows. International Journal of Heat and Fluid Flow. **26**(4)(2005): p. 530–546.